RSC Advances

PAPER

View Article Online
View Journal | View Issue

Cite this: *RSC Adv.*, 2025, **15**, 36981

Influence of praseodymium(III) chloride on corrosion resistance of AS1020 steel in an environment containing chloride ions and carbon dioxide

Casen Panaitescu, †[a] Thi-Bich-Ngoc Dao, †[bc] Cam-Tu Hoang-Ngoc, [bc] Nhi Ngoc Nguyen, [bc] Trung T. Pham, [d] Minji Kim, [e] Tuan Le Minh [f] and Thanh Liem Huynh *[bc]

Rare earth salts (RESs) are considered one of the good choices for anticorrosion due to their high inhibition efficiency *via* the suppression of oxygen reduction reactions. In this work, praseodymium chloride ($PrCl_3$) was used as a potential inhibitor that can become a promising candidate for mitigating mild steel corrosion in environments rich in chloride and carbon dioxide. The results of electrochemical and surface analyses indicated that mild steel was protected from corrosion in a CO_2-saturated sodium chloride solution throughout 72 hours immersion when $PrCl_3$ was added to the solution. This was evidenced through considerably reduced corrosion current density, increased protective and charge transfer resistances, especially, random redistribution of minor anodes, as well as less corrosion-induced damages on the steel surfaces. Tafel extrapolations were applied to estimate the inhibition efficiency of $PrCl_3$, achieving the highest value of 96.33 ± 0.47 % at 2.4 mM $PrCl_3$. This positive result is primarily attributed to the formation of the barrier layer from praseodymium oxides and hydroxides in combination with iron(II)-based products. Based on these findings, this work recommends a potential inhibitor for mitigating mild steel corrosion in aqueous media containing carbon dioxide and chloride ions.

Received 15th July 2025
Accepted 11th September 2025

DOI: 10.1039/d5ra05060j

rsc.li/rsc-advances

1. Introduction

The progress of human society is intricately tied to advancements in equipment and technology, both significantly affected by the materials utilized. Nevertheless, the inevitability of damage, particularly corrosion, poses a primary challenge. Mild steel, valued for its ease of fabrication and affordability, is used in a wide range of applications.[1,2] This is notably evidenced in the construction of marine projects, including port facilities, petrochemical installations, and ship structures, where steel and reinforced concrete take precedence.[3] The imperative lies in safeguarding these materials against environments laden with chloride ions and carbon dioxide (CO_2), which are byproducts of both natural surroundings and vehicular emissions – primary contributors to sweet corrosion, pitting corrosion, and transgranular cracking.[4,5] Since 90% of the world's trade in raw materials and completed goods depends on the shipping industry,[6] stringent measures are essential to control potentially detrimental factors. In instances where their indispensability cannot be altered, the need for protection becomes critical.

CO_2 exists in various industry systems, such as oil and gas, CO_2 capture and storage, and enhanced recovery processes. However, its significance is unfortunately accompanied by adverse effects on Earth's climate and a heightened risk of severe corrosion in aqueous environments.[7,8] Notably, carbonic acid-induced corrosion presents more substantial challenges than that caused by strong acids at equivalent pH levels,[9] leading to significant damage and increased risks in the use of materials and equipment. Fueled by the above core objectives, increasing efforts are being directed towards addressing the challenges through corrosion-based methodologies such as material selection,[10] protective coatings,[11] and corrosion inhibitors.[12–14] Although complete prevention of the corrosion process is unattainable, these methods substantially reduce corrosion rates, averting losses of approximately 20–30%.

[a]*Department of Petroleum Geology and Reservoir Engineering, Petroleum-Gas University of Ploiesti, Ploiesti 100680, Romania*

[b]*Future Materials & Devices Lab., Institute of Fundamental and Applied Sciences, Duy Tan University, Ho Chi Minh City 70000, Vietnam. E-mail: huynhthanhliem@duytan.edu.vn*

[c]*Faculty of Civil Engineering, Duy Tan University, Danang 55000, Vietnam*

[d]*Namur Institute of Structured Matter (NISM), Department of Physics, University of Namur, 61 Rue de Bruxelles, Namur B-5000, Belgium*

[e]*Department of Semiconductor Process, Korea Polytechnic University, 56, Munemi-ro 448beon-gil, Bupyeong-gu, Incheon, 21417, Republic of Korea*

[f]*Institute of Science and Technology for Energy and Environment, Vietnam Academy of Science and Technology, Ho Chi Minh City 70000, Vietnam*

† Contributed equally to this work and these authors can put as the first author in the CV.

Corrosion inhibitors emerge as an effective method to prevent the long-term corrosion of materials in general, which is widely used in the petrochemical and mechanical manufacturing industries.[14–17] These inhibitors facilitate the formation of a protective film, influencing corrosion inhibition through chemical bonds between metals and natural and/or synthetic organic inhibitor molecules.

In fact, inhibitors form ordered molecular structures on metal surfaces, similar to surfactants that create monolayers or bilayers, and demonstrate the ability to slow down material corrosion when introduced into the environment at minimal concentrations. To date, inhibitors derived from inorganic, organic, and inorganic–organic compounds have been developed and optimized for mitigating CO_2-induced corrosion of steel. Among them, organic inhibitors are considered an effective approach due to their ready availability, sustainability, effective costs, easy extraction, high performance, and especially non-toxicity. The typical organic compounds can be classified as imidazoline-based compounds (or derivatives),[18–24] non-imidazoline inhibitors,[25–27] polymeric inhibitors,[28–30] and natural inhibitors extracted from plant components[31] such as *Calotropis procera* leaves,[32] *Ginkgo biloba* fruit,[33] *Stachys scardica* H. leaves,[34] and *Syzygium malaccense* DNA.[35] Recently, in a study by Zhang and Xu,[26] two synthetic amino acid derivatives, namely 2-phenylthiazolidine-4-carboxylic acid (PTCA) and 2-(thiophene-2-yl)thiazolidine-4-carboxylic acid (TTCA), demonstrated corrosion inhibition effects on carbon steel in a CO_2-containing environment. Using a chemical modification method, inhibition effects were observed at a concentration of 0.8 mM, Cunha *et al.*[25] explored the use of furfural derivatives as a green corrosion inhibitor for mild steel in CO_2-saturated aqueous solutions. Their research highlighted that the inhibition mechanism involves the transformation of FeOH–OH surface species into a protective, surface-blocking film, thereby enhancing corrosion resistance, achieving an inhibition efficiency of 90.2% after 72 hours. These findings underscore ongoing efforts to identify environmentally friendly, reliable, and sustainable organic or inorganic inhibitors capable of minimizing and controlling steel corrosion with minimal use of the additive. However, the effectiveness of organic compounds, typically imidazoline and its derivatives, in inhibiting localized corrosion of carbon steel in CO_2-rich environments, remains uncertain.[36,37]

Furthermore, Anadebe *et al.*[38] showcased the anti-corrosion effectiveness of synthesized Ni-MOF in sweet corrosive environments, achieving a remarkable inhibition efficiency of 94% for X65 steel. Extensive research has been focused on developing environmentally friendly corrosion inhibitors for steel in CO_2-rich environments, with rare earth-based compounds emerging as promising options due to their unique physicochemical properties and high inhibition efficiency.[39,40] For instance, in 2014, Forsyth and colleagues demonstrated that a series of rare earth-based organic compounds serve as effective corrosion inhibitors for both steel and aluminum alloys.[41] These substances form nanometer-thick films with complex structures that effectively reduce electrochemical reactions responsible for increasing the corrosion rate. Unfortunately, the synthesis involved several steps,[42] and the resulting protective film, characterized by crystalline particle coverage, exhibited non-uniform distribution on the steel surface,[39,40] thereby raising concerns about the reliability and scalability of its applications. Alternatively, rare earth elements can exert physic-metallurgical effects on steel, enhancing its self-corrosion resistance and reducing the current density of electrochemical corrosion. This is achieved through their strong chemical activities, facilitating interactions with elements such as O and S in molten steel.[43] Xing *et al.* noted that the addition of rare earth elements through coating enhances the stability and resistance to electrochemical corrosion for grade 304 stainless steel in a 3.5 wt% NaCl solution.[44] Zhang and colleagues demonstrated that rare earth elements, when introduced *via* alloying, improve the microstructure and overall properties of alloys by enriching contact surfaces and hampering the formation and development of undesirable phases.[45] Collectively, these findings suggest promising corrosion-inhibitory properties of rare earth elements, which have been applied through various methods. These investigations indicated that rare earth salts could be potential inhibitors, offering viable alternatives to traditional inorganic compounds such as arsenic-, arsenate-, chromate-, dichromate-, and nitrate-based formulations, which have unsightly influences on the environment and human health.[46] Other works reported that lanthanide salts achieve a high degree of inhibition performance for aluminum alloys *via* the retardation of the cathodic process in electrochemical corrosion reactions[47–49] *via* the hydrolysis process of rare earth(III) cations. These studies also propose lanthanide salts as ecological alternatives to chromate-based inhibitors, with praseodymium chloride ($PrCl_3$) demonstrating its effectiveness in corrosion inhibition in NaCl media.[50,51] Moreover, recent toxicokinetic analyses have provided valuable safety profiles in rodent models,[52] which provide a strong rationale for selecting $PrCl_3$ as a promising candidate for further investigation as an environmentally friendly corrosion inhibitor. Furthermore, this salt has not yet been explored for corrosion protection of carbon steel in carbon dioxide-rich environments. Accordingly, the present work proposes the use of $PrCl_3$ to investigate its inhibitory performance on mild steel as immersed in a CO_2-saturated sodium chloride solution. The study will primarily focus on examining corrosion resistance from electrochemical techniques, supplemented by surface characterization methods to elucidate the role of $PrCl_3$ in the development of protective mechanisms against corrosion.

2. Experimental section

2.1. Materials

All chemicals in this study, including praseodymium(III) chloride hydrate ($PrCl_3 \cdot xH_2O$), ethanol (C_2H_5OH), and sodium chloride (NaCl), were sourced from Merck KGaA and used directly without further purification. Mild steel, classified as plain-carbon steel with low carbon content, was employed in this study and its chemical composition is detailed in Table 1.

The mild steel was shaped into a cylindrical bar with a diameter of 16 mm and then coated with an outer layer of

Table 1 Mild steel compositions determined by optical emission spectroscopy (OES)

	Chemical elements (wt%)														
	C	Mn	Si	S	P	Ni	Cr	Mo	Cu	V	Nb	Ti	Al	B	Fe
AS1020	0.16	0.73	0.21	0.01	0.02	<0.01	0.03	<0.01	<0.01	0.01	<0.01	<0.01	<0.005	<0.005	Bal.

epoxy to retain fixed exposed surface area. The epoxy resin utilized was a two-component system comprising resin A and a hardener mixed at a ratio of 3/1 of resin and hardener. To ensure the accuracy of all electrochemical experiments, a crucial step involving the removal of corrosive products and scratches from the steel surface is necessary. Therefore, before all experiments, steel surfaces were polished with silicon carbide papers with different grits of 120, 600, 1000, and 2000. Subsequently, surface finishes were cleaned with distilled water and ethanol and finally dried using a hairdryer.

2.2. Surface analysis

To investigate the morphological changes induced by $PrCl_3$, various analytical techniques were employed to assess its impact on the mild steel surface as immersed in a solution with the inhibitor at different concentrations. A field emission scanning electron microscope (FE-SEM), particularly Hitachi S-4800 FE-SEM, was used to observe the morphologies and elemental distribution on the mild steel surface after immersion in the corrosive solution with different $PrCl_3$ concentrations. At other neighboring positions for samples containing 0 and 2.4 mM $PrCl_3$, energy-dispersive X-ray spectrometer (EDS) detector was performed and reflected the mapping of characteristic elemental distribution. Finally, X-ray photoelectron spectroscopy (XPS) was conducted for precise examination and identification of peaks corresponding to the presence of Fe, C, O, Cl, and Pr on the mild steel surface.

2.3. Electrochemical analysis

The electrolyte solution consists of 0.01 M NaCl, into which $PrCl_3$ was added at different concentrations of 0.0, 0.4, 1.2, and 2.4 mM. Prior to experiments, each solution was aerated with high-purity CO_2 gas (99.999%) for one hour and continuous CO_2 bubbling was maintained throughout the experimental procedure to ensure saturation (pH $\sim$ 4). All electrochemical assessments were conducted on a three-electrode system at an ambient temperature of approximately 25 $\pm$ 1 °C using a VSP potentiate system (BioLogic Scientific Instruments). The three-electrode system consisted of mild steel specimens serving as the working electrode (WE), a counter electrode (CE) with titanium mesh, and a Ag/AgCl reference electrode (RE) filled with saturated KCl. Firstly, the open circuit potential (OCP) was monitored for 2 hours before each electrochemical test to ensure that the system remains stable. Secondly, electrochemical impedance spectroscopy (EIS) was carried out over a frequency range of 10 kHz to 10 mHz with a sinusoidal perturbation amplitude of 10 mV for 72 h. Continuous EIS monitoring throughout the 72 hour immersion allowed capturing the time-dependent evolution of the electrochemical behavior, providing a comprehensive understanding of the inhibitor's performance and stability over both the short and prolonged exposures. These EIS results obtained were represented and fitted using the Origin program and Zsimpwin software, respectively. In addition, after 72 hours of OCP, potentiodynamic polarization (PD) was set up at a potential ranging from −250 mV *vs.* OCP to 0.1 $mV_{Ag/AgCl}$ at a scan rate of 0.166 mV s^{-1} according to ASTM G5-94.

Furthermore, to characterize localized corrosion inhibition, a wire beam electrode (WBE) test was performed following a previously reported procedure.[13,53] Particularly, after 1 h of initial corrosion in the blank solution, $PrCl_3$ inhibitor (0.4, 1.2, and 2.4 mM) were injected into the WBE testing cell every 24 h, while continuous CO_2 purging was maintained.

3. Results and discussion

3.1. Surface morphology analysis results

The morphology of steel surfaces as immersed in the investigated solutions for 72 hours was analyzed by SEM, and the elemental distribution was identified *via* both SEM and EDS mapping analyses. Fig. 1 presents the SEM images of the corroded surfaces that are quite different between the uninhibited and inhibited surfaces. Fig. 1(a) shows that the surface was severely corroded in the blank solution. In the investigated solution with pH $\sim$ 4, mild steel acts as an active material that was easily dissolved to Fe^{2+} ions, releasing into the solution and generating electrons used for hydrogen evolution at the cathodic sites. Technically, aggressive corrosion occurrs on unstable intermetallic phase, such as pearlite sites, while cementite phase (Fe_3C) was less affected by the corrosion reactions due to its durability and structural stability, as shown in Fig. 1(a). However, slight corrosion at pearlite sites can be seen on the inhibited steel surfaces and the corrosion levels decreased as the $PrCl_3$ concentrations in the electrolyte increased, as presented in Fig. 1(b) and (c). Importantly, Fig. 1(d) shows some lightly pock-marked locations due to the gentle etching on the steel surface exposed to the CO_2-saturated 0.01 M NaCl solution containing 2.4 mM $PrCl_3$. Furthermore, the inhibited surfaces likely have a thinner surface film formed *via* Pr^{3+} hydrolysis, which facilitates the formation of the stable protective layer composed of praseodymium oxides/hydroxides and iron products. The distribution of elements in the protective layer was characterized by SEM/EDS mapping, as shown in Fig. 2. The results showed a relatively rough and heterogeneous surface morphology, indicative of surface modification and possible formation of corrosion products and protective deposits. The mixed-elemental distribution indicates that

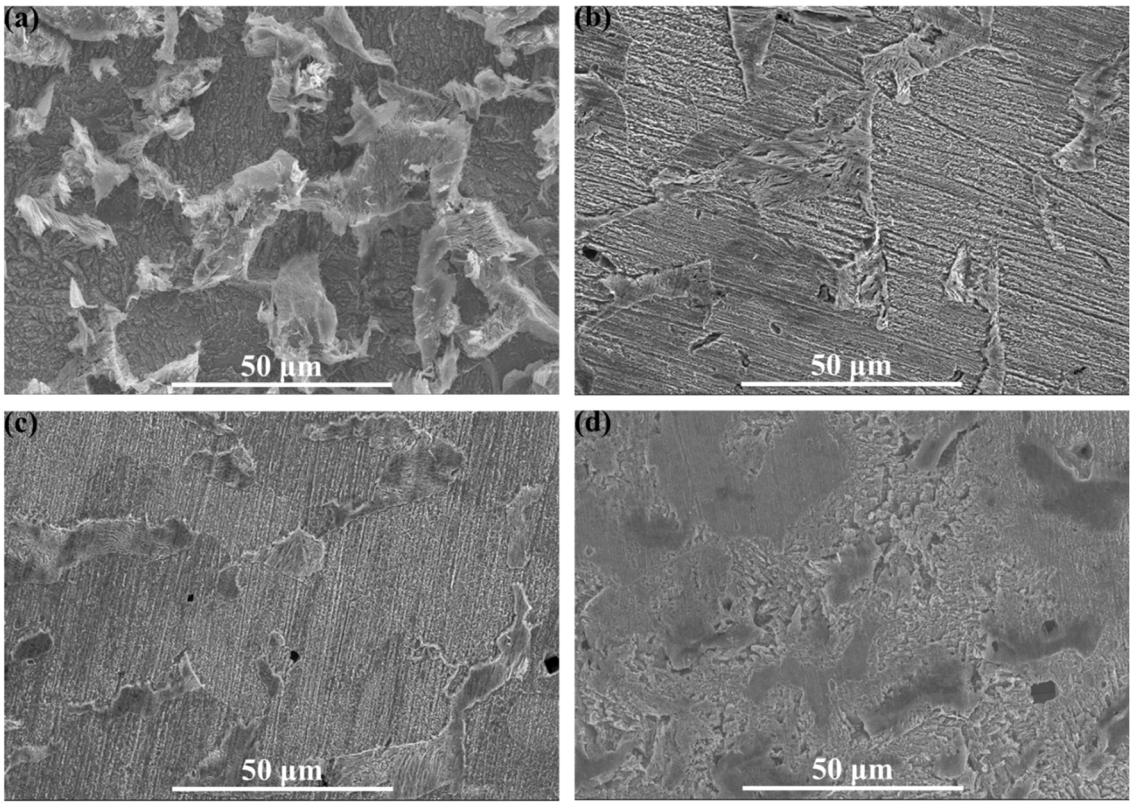

Fig. 1 Scanning electron microscopy images showing morphologies after 72 hours corrosion in a CO_2-saturated 0.01 M NaCl solution with: (a) 0.0, (b) 0.4, (c) 1.2, and (d) 2.4 mM $PrCl_3$ addition.

abundant Fe, Pr, and O are uniformly distributed over the inhibited surface. This mapping also reveals the presence of Fe as the major component, with significant oxygen (O) signals, suggesting the formation of oxide layers. In addition, carbon (C) element contributes only marginally to the thin layer formed on the steel surface. During corrosion, the ferrite and pearlite, which are generally more electrochemically active, undergo preferential dissolution. This process exposes the more corrosion-resistant cementite (Fe_3C), allowing carbon from this phase to be detected in the spectra. Such selective phase degradation is consistent with microstructural evolution observed in low-carbon steels in corrosive environments.[54] Additionally, chlorine (Cl) was detected at lower concentrations, likely originating from the corrosive medium and subsequently incorporated into the corrosion products. These ions can accelerate localized corrosion processes, particularly pitting,

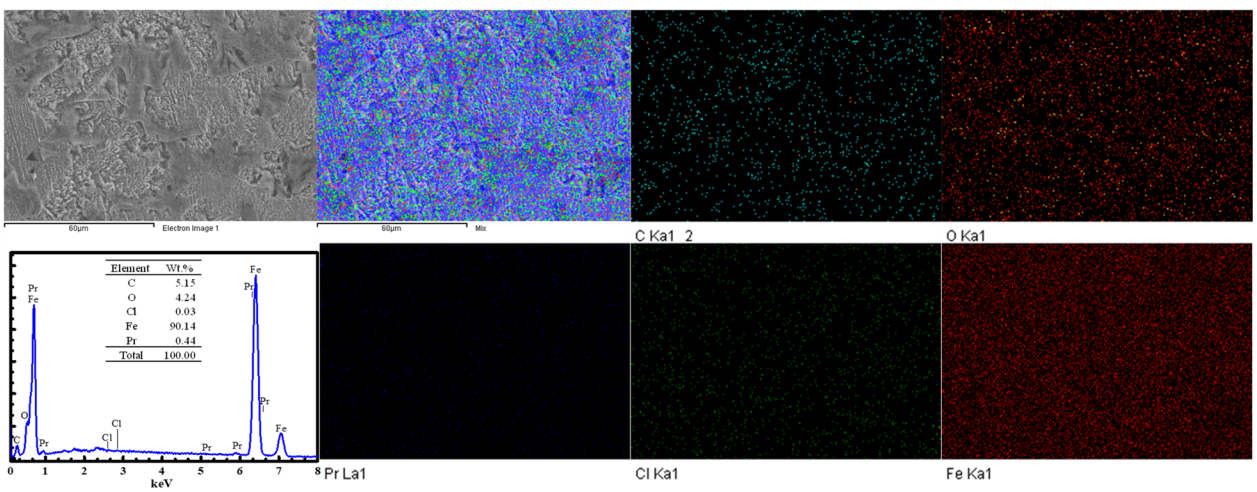

Fig. 2 SEM/EDS mapping of the substrate surface after 72 hours corrosion in a CO_2-saturated 0.01 M NaCl solution with 2.4 mM $PrCl_3$ addition.

and may become embedded within corrosion layers as the reaction progresses. Furthermore, Pr signals were consistently detected across the surface alongside Fe, O, C, and Cl, indicating effective adsorption and deposition of Pr ions onto the mild steel substrate. Moreover, the EDS spectrum shows strong Fe peaks along with clear Pr peaks, confirming the incorporation of rare earth elements into the surface layer.

To clarify the chemical state of elements on formed thin layer of mild steel after 72 hours immersion, XPS was conducted to the investigated solutions containing 0.0 and 2.4 mM $PrCl_3$. Fig. 3(a) presents the XPS spectra and confirms the evident existence of different elements, including Fe 2p, C 1s, and O 1s in the low-resolution spectra. Importantly, the Pr 3d peak was only observed for the inhibited mild steel surface, demonstrating the participation of $PrCl_3$ on the interface processes of mild steel in corrosive solution. Fig. 3(b) presents the high-resolution XPS spectrum of Fe 2p with Fe $2p_{1/2}$ and Fe $2p_{3/2}$ at binding energies around 723.8 and 710.3 eV, respectively. More specifically, Fe(II)Fe $2p_{1/2}$ and Fe(III)Fe $2p_{3/2}$ satellites positioned around 733.1 and 719.1 eV are observed for both the uninhibited and inhibited surfaces. However, there are less intensities of Fe peaks observed on the inhibited surface reflecting the reducing of corrosion products when $PrCl_3$ was added in corrosive solution. Specially, the peak of Fe at around 706.7 eV could be assigned to Fe from the mild steel substrate as immersed in the blank solution, probably induced by the formation of a thin corrosion product layer on the steel surface. This process can cause the rapid release of Fe^{2+} to the solution, resulting in the Fe exposure of the steel substrate after 72 hours corrosion in the CO_2-saturated 0.01 M NaCl solution. Furthermore, peaks of carbon products can be observed at around 710.5 and 723.9 eV, as shown in Fig. 3(b), corresponding to the COO^- peaks of C 1s spectra at 288.3 eV in Fig. 3(c) and O 1s spectra at 532.0 eV in Fig. 3(d), respectively. Importantly, the Fe signals of Fe_2O_3, FeO, and α-FeOOH products at around 726.3 and 713.8 eV, as shown in Fig. 3(b), correspond to O^{2-} and OH^- peak at 531.1 and 729.7 eV of O 1s spectra in Fig. 3(d). Fig. 3(c) shows the narrow scan of C 1s with three main peaks, namely a peak at 288.3 eV assigned to iron carbonate and two peaks at 286 and 284.7 eV corresponding to C–O and C–C of the C-based products from the original steel structure. Fig. 3(d) indicates three O 1s peaks at around 532.0, 729.7, and 531.1 eV, which are consistent with COO^-, OH^-, and O^{2-} present in carbonates, hydroxides, and oxides on the mild steel surface in all of results, while Fig. 3(e) shows the limited occurrence of Cl-based products, as evidenced through low peaks of Cl 1s in all results. Importantly, Pr 3d peaks shown in Fig. 3(f) with high intensity of Pr $3d_{3/2}$ and Pr $3d_{5/2}$ at binding energies of around 943.1 and 934.1 eV, respectively, are consistent with the reported values for praseodymium oxides and hydroxides incorporating iron products leading the ligh shift of OH^- and O^{2-} in O 1s spectra.[50] The dominant Pr $3d_{5/2}$ peak position and line shape indicate the presence of Pr^{3+} species, most likely present as Pr_2O_3 or $Pr(OH)_3$ deposited on the steel surface during the inhibition process. In this corrosive environment, the persistence of intense Pr 3d signals suggests that the Pr-based compounds effectively adsorb and form stable surface. This correlation between Pr chemical states and the CO_2-saturated 0.01 M NaCl environment highlights the ability of Pr salts to form robust protective layers, thereby enhancing corrosion resistance under these conditions.

3.2. Electrochemical analysis results

Fig. 4 compares the polarization results of the mild steel in a CO_2-saturated NaCl environment. The curves show clear

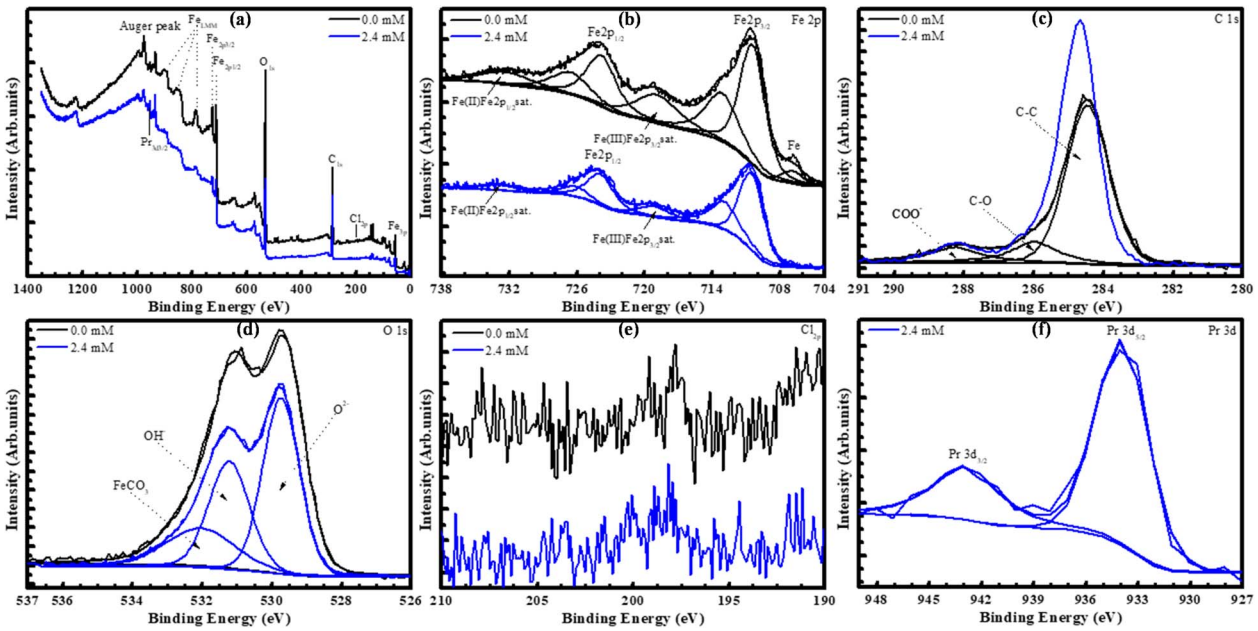

Fig. 3 Survey and narrow XPS spectra of MS surfaces immersed in a CO_2-saturated 0.01 M NaCl solution with 0.0 and 2.4 mM $PrCl_3$ addition: (a) survey, (b) Fe 2p, (c) C 1s, (d) O 1s, (e) Cl 2p, and (f) Pr 3d spectra.

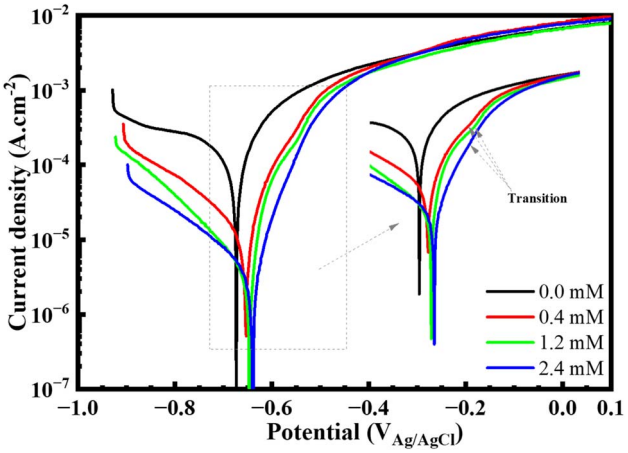

Fig. 4 Represented potentiodynamic polarization of mild steel after 72 hours corrosion in CO_2-saturated 0.01 M NaCl solutions containing different $PrCl_3$ concentrations.

differences between the uninhibited and inhibited systems, indicating a significant influence of $PrCl_3$ on the electrochemical characteristics of the mild steel in the CO_2-saturated sodium chloride environment. For the uninhibited system, results indicates that a plateau of applied potential ranging in the cathodic branch ($<E_{corr}$) reflects a cathodic limiting current density, suggesting the effect of diffusion in corrosion process of mild steel. This phenomenon is consistent with previous work by Aria and colleagues on a mild steel surface.[55,56] Furthermore, there is not any linear behavior of the anodic current density in the PD result of the uninhibited specimen, indicating the dissolution of mild steel surface in anodic branch consistent with the SEM image shown in Fig. 1(a). It suggests that mild steel acts as an active material in the CO_2-saturated NaCl solution. In the case of the inhibited systems, the similar shapes are observed on both the cathodic and anodic branches at all $PrCl_3$ concentrations, suggesting that anodic and cathodic reaction mechanisms remained unchanged for all inhibited systems. The inhibition effect is primarily attributed to the reinforcement of the oxide/hydroxide (as demonstrated in XPS spectra) layer formed through the hydrolytic reaction of praseodymium ions from the inhibited system. A similar cathodic polarization behavior was observed in all results of the inhibited system, but without the plateau associated cathodic limiting current density as the blank sample. This indicates that Pr^{3+} ions are highly electroactive and strongly affect the cathodic charge transfer process of mild steel in the CO_2-saturated NaCl solution, resulting in an overall decrease in corrosion current densities. At this stage, the inhibition of cathodic process is much pronounced due to the Pr^{3+} hydrolysis that facilitates the precipitation of $Pr(OH)_3$ and Pr_2O_3 products. This is relatively consistent with XPS observations shown in Fig. 3(a) and (f). Thus, as $PrCl_3$ concentrations in the electrolyte increase, its inhibition performance significantly increases, primarily driven by the higher stability of the $Pr(OH)_3$ and Pr_2O_3 precipitation. However, anodic current densities in the polarization curves of the inhibited system indicate a significant influence of the inhibitor on electrochemical processes, as evidenced by a substantially reduced current density compared to the uninhibited system. This further supports the formation of a stable protective layer on the mild steel surface, retarding the anodic reaction. At low $PrCl_3$ concentrations of 0.4 and 1.2 mM, the transition region occurs at around -0.54 $V_{Ag/AgCl}$, which is not observed in the case of 2.4 mM $PrCl_3$. Furthermore, the values of anodic current densities begin to slightly increase with more positive anodic potential, which agrees with the work done by Linter *et al.*[57] Additionally, the stability of the protective layer could be attributed to iron hydroxides and oxides in combination with other products (Fig. 2 and 3), which are likely $Pr(OH)_3$ and Pr_2O_3 precipitations. Therefore, both anodic and cathodic corrosion current densities reduce "hand in hand", resulting in a significant decline in overall corrosion current density. This phenomenon demonstrates that $PrCl_3$ is a mixed corrosion inhibitor, with predominant cathodic inhibition. Table 2 shows the corrosion parameters, including i_{corr}, E_{corr}, β_a, and $-\beta_c$, extracted through PD curves by Tafel extrapolation, where i_{corr} was calculated by means of duplicate or triplicate results. The fitted errors are minimized *via* the movement of anodic and cathodic lines within $\pm$100 mV from corrosion potential (E_{corr}). The results indicate that the addition of higher concentrations of $PrCl_3$ slightly leads to an increased corrosion potential (E_{corr}) and strongly decreased corrosion current density (i_{corr}), indicating a greater inhibition performance. In the blank sample, the anodic dissolution of steel is fast and uncontrolled, and hydrogen evolution and bicarbonate/carbonate reduction occur rapidly, giving a steep slope of anodic (159 mV per decade) and cathodic curves. With $PrCl_3$ addition, Pr^{3+} hydrolyzes to $Pr(OH)_3/Pr_2O_3$, co-depositing with Fe products to form a protective film. This layer blocks active cathodic sites and hinders proton reduction and bicarbonate-to-carbonate conversion, leading to slow Fe^{2+} release. As a result, the kinetics of hydrogen evolution and metal dissolution becomes more activation-controlled, hence lower β_a and $-\beta_c$ values. The fact that both slopes reduce steadily with the concentration also suggests that film growth becomes denser and more adherent with time and concentration, making charge transfer more difficult in both directions.

Fig. 5 and 6 present the Nyquist and Bode (phase angle *vs.* frequency) plots for EIS results for 72 hours of immersion in the CO_2-saturated NaCl solution containing different $PrCl_3$ concentrations. The Nyquist plots show a single semicircle corresponding to the solution and charge transfer resistances at high and low frequencies,[58] respectively. However, in blank systems, the Nyquist plots at low frequencies exhibit a distinct inductive loop, which is related to intermediate species involved in the adsorption processes. Nevertheless, this inductive behavior does not significantly influence the total resistances.[58,59] Evidence of the decrease in solution resistance and the increase in the diameter of semicircles is observed when $PrCl_3$ concentrations increased from 0 to 2.4 mM in the investigated solution. In the blank solution, mild steel has relatively small impedance values, indicating an accelerant corrosion reaction. The slight increase in impedance values in some first

Table 2 Corrosion parameters of AS1020 steel after 72 hours exposition in saturated CO_2 0.01 M NaCl solutions containing different $PrCl_3$ concentrations, as observed from the PD curves in Fig. 4

Concentration (mM)	E_{corr} ($mV_{Ag/AgCl}$)	i_{corr} ($\mu A\ cm^{-2}$)	β_a (mV per decade)	$-\beta_c$ (mV per decade)	Inhibition efficiency (%)
0.0	−684	163.8 ± 1.38	159	605	—
0.4	−648	18.62 ± 6.27	110	375	88.64 ± 3.83
1.2	−644	11.23 ± 1.32	94	277	93.15 ± 0.81
2.4	−638	6.02 ± 0.78	52	185	96.33 ± 0.47

hours can be due to the formation of corrosion products composed of main iron oxides/hydroxides/carbonate products, while this decreased value could be assigned to the promotion of the steel dissolution. The solution resistance decreases with the increase in immersion time, ensuring an enrichment of ions produced from steel dissolution in the investigated solution. Regarding the inhibited systems, there is a significant reduction of solution resistance due to $PrCl_3$ addition and a strong increase in semicircle diameters caused by the protective film formation. The semicircle diameters of EIS results in the corrosive solutions containing 0.4 mM and 1.2 mM $PrCl_3$ still steadily increase and remain stably up to 72 hours of immersion, suggesting the promoted corrosion resistance. Noteworthy, the semicircle diameters of EIS results increase steadily up to 32 hours with 2.4 mM $PrCl_3$ in the CO_2-saturated NaCl solution. After that, these semicircles remained stable until 48 hours and then slightly decreased over immersion hours, but still reach very high impedance values. It indicated the thin film

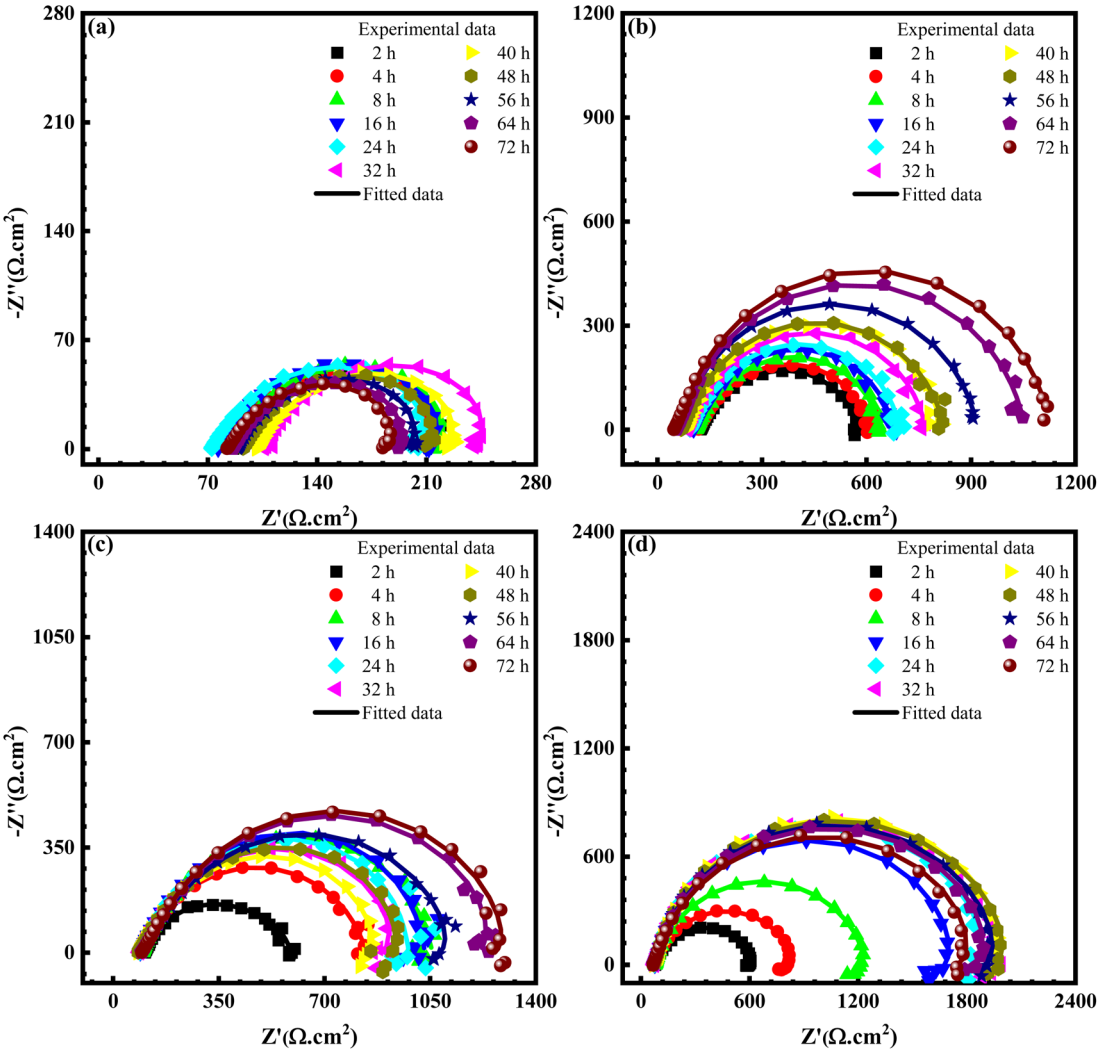

Fig. 5 Nyquist plots representing the experimental and fitted EIS results of mild steel during 72 hours corrosion in CO_2-saturated 0.01 M NaCl solutions with (a) 0.0, (b) 0.4, (c) 1.2, and (d) 2.4 mM $PrCl_3$ addition.

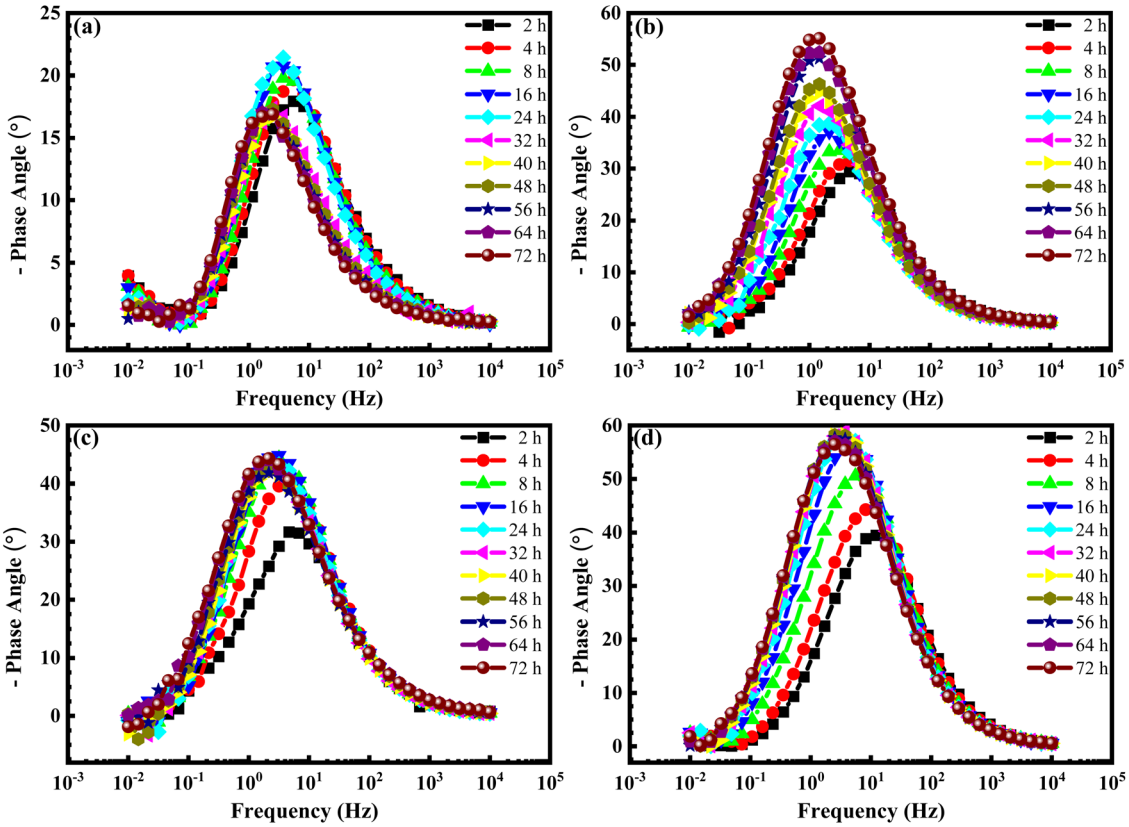

Fig. 6 Represented Bode plots of mild steel during 72 hours corrosion in CO_2-saturated 0.01 M NaCl solutions with (a) 0.0, (b) 0.4, (c) 1.2, and (d) 2.4 mM $PrCl_3$ addition.

layer is well protected, but may be present to be desorped slighly of Pr and/or Fe(II)-based compounds. The variation in the phase angle in Bode plots (Fig. 6) provides valuable insights into the interfacial behavior and the stability of the protective film formed on mild steel. In the blank system, the peaks of phase angle only reach approximately 20°, indicating a highly porous and defective surface with limited capacitive behavior. Such low values reflect that charge transfer processes dominate, consistent with rapid corrosion activity. Upon the addition of $PrCl_3$, the phase angle peak values increase progressively with inhibitor concentration, reaching nearly 60° at 2.4 mM. This increase implies that the interfacial layer behaves more like a capacitive barrier, where the charge transfer process is effectively suppressed by the formation of a Pr-based protective film. Importantly, the broadening of the phase angle plateau over the intermediate frequency region reflects that the film is not only capacitive but also stable over a wide time constant distribution, which is typical for a compact and adherent layer. Moreover, after prolonged immersion (48–72 h), the shape of the phase angle curves remains unchanged at higher inhibitor concentrations, indicating that the protective film maintains its structural integrity without significant delamination or degradation. Thus, the phase angle variations are closely linked to the protective film characteristics with a compact, capacitive, and durable Pr-based film, demonstrating by the higher values and broader plateaus, and even this film is also stable over time.

The EIS parameters were extracted from a proposed equivalent circuit given in Fig. 7(a), and the accuracy of fitted parameters were determined based on the traces between the experimental and fitted data, as well as percent error and chi-square (χ^2) values. The proposed equivalent circuits in Fig. 7(a1) and (a2) are suitable for fitting EIS data flexibly, ensuring small differences in the experimental and fitted data, less than 100% errors and 10^{-4} χ^2 values. The extracted data are summarized in Tables S1–S4. Fig. 7(b) presents the average values of R_{ct} limited at low frequencies in EIS measurements. Very small R_{ct} values slightly increase for first 8 hours of immersion and then slightly decrease, suggesting high corrosion reactions on the mild steel surface as exposed to the CO_2-saturated NaCl solution. At a low concentration of the inhibitor, specifically 0.4 mM $PrCl_3$, the R_{ct} value increases significantly with immersion time, indicating the strong protective effect of the inhibitor at this concentration. At 1.2 mM concentration of $PrCl_3$ in the CO_2-saturated NaCl solution, the R_{ct} values rise considerably for the first 28 hours, and then slightly decrease in the subsequent hours. Afterward, they increase again and remain stable at 64 hour until the end of the test. This behavior could be attributed to the instability of the thin film, which is subsequently restored by the inhibitor molecules in the corrosive solution. Meanwhile, the R_{ct} values of the CO_2-saturated NaCl solution containing 2.4 mM $PrCl_3$ increase over immersion time and reach the highest values in comparison with

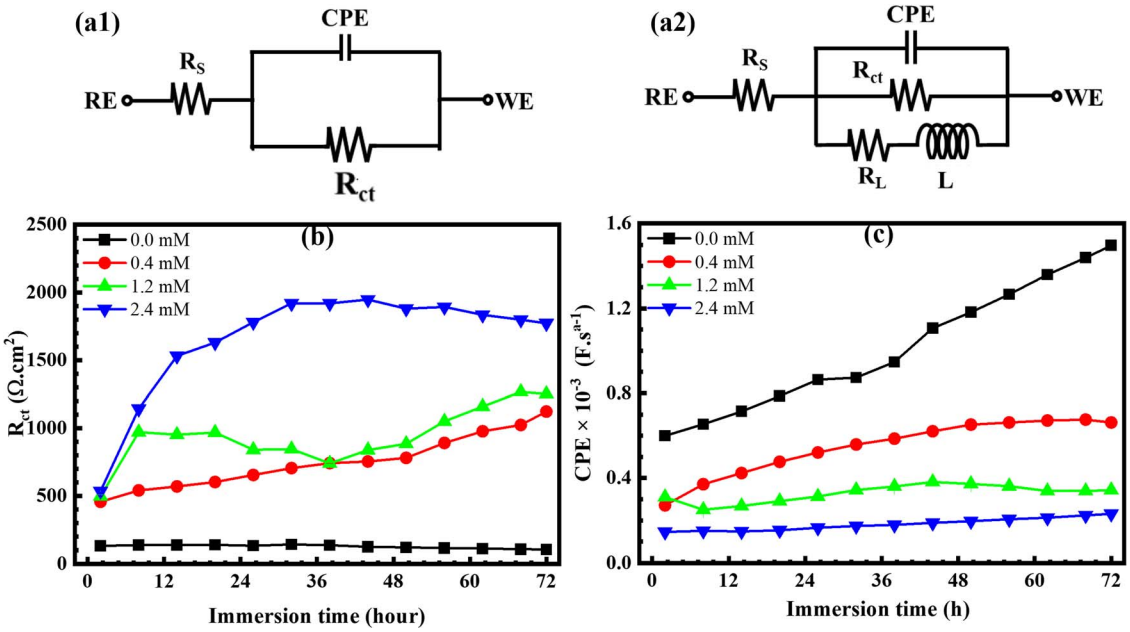

Fig. 7 (a) Proposed equivalent circuit and effect of $PrCl_3$ concentrations and immersion time on (b) charge transfer resistance and (c) double layer CPE magnitudes.

other concentrations, suggesting improved inhibition performance. Furthermore, the influence of aggressive ions in the investigated solution on the steel substrate could be assigned to the CPE magnitude values, as given in Fig. 7(c). The result shows the highest value for the uninhibited specimen, indicating the limit formation of the corrosion products, and instead, the steel surface became more corroded, as shown in the SEM and XPS results. Furthermore, the decrease in the CPE magnitude for inhibited surfaces indicates small values and it decreases with the increase in $PrCl_3$ concentration, as shown in Fig. 7(c). The obtained results show that the mild steel surface is covered by the dense and improved integrity and adhesion of the protective layer, as demonstrated in SEM/EDS and XPS results in Fig. 1–3, as well as the polarization curve. This causes high corrosion resistance of mild steel in the investigated solution.

To characterize the localized corrosion resistance and predominant cathodic inhibition of $PrCl_3$, the current distribution over the spontaneously corroding mild steel surface was characterized by WBE, and the results are given in Fig. 8. The current distribution map of the mild steel surface in Fig. 8(a) was recorded after 24 h taking in the CO_2-saturated NaCl solution, that shows high current values of both cathode and anode sites, corresponding to center and borderland of the map, respectively. This imbalance between 2 electrodes can lead to severe localized corrosion. Importantly, a large difference between maximum cathodic and anodic current values was observed, indicating a high corrosion reaction of mild steel in the investigated solution. Fig. 8(b)–(d) shows the map of current distribution over the WBE surface after 24 h immersion time for each condition. Anodic and cathodic currents are randomly distributed on the inhibited surface with a significant decrease in current values when the $PrCl_3$ concentration is increased from 0.4 to 2.4 mM. Importantly, the difference between maximum cathodic and anodic current values of the anodic and cathodic distribution in a random manner is very small and significantly decreases with the increase in $PrCl_3$ concentration. This is attributed to a less active steel surface, reflecting a great inhibition of $PrCl_3$ for localized corrosion on the mild steel in the CO_2-saturated NaCl solution.

3.3. Corrosion and inhibition mechanisms

Based on surface analysis and electrochemical experiments, the electrochemical corrosion of mild steel could initially appear at the lacuna sites on the steel surface structure, particularly at the boundary between the pearlite and cementite sites. This phenomenon could result in a change in the local pH on the steel surface. The steel, mainly iron, could be continuously dissolved with increasing immersion time. As a result, a main part of Fe ion (only Fe^{2+} at pH $\sim$ 4)[60] release will be enriched in the investigated solution and the other small part of Fe ions will produce the corrosion scale formed on the steel surface. These processes could result in severe corrosion in the pearlite regions and cause limited damage to the cementite sites (Fig. 1(a)). In addition, the thin corrosion scale layer mainly consists of Fe_2O_3, FeO, and α-FeOOH formed on the steel surface, as shown in Fig. 1(a), and confirmed by the Fe 2p and O 1s peaks in Fig. 3. Fortunately, when mild steel is exposed to the investigated solution containing Pr^{3+} ion, the electrochemical corrosion reactions of mild steel surface are significantly hindered by a precipitation of praseodymium oxide/hydroxide (stable +III state) and can exist the +IV state due to the complex oxidation occuring in corrosion processes as well as the preferred oxidation states of this element.[61] The Pr^{3+} ions are released by the

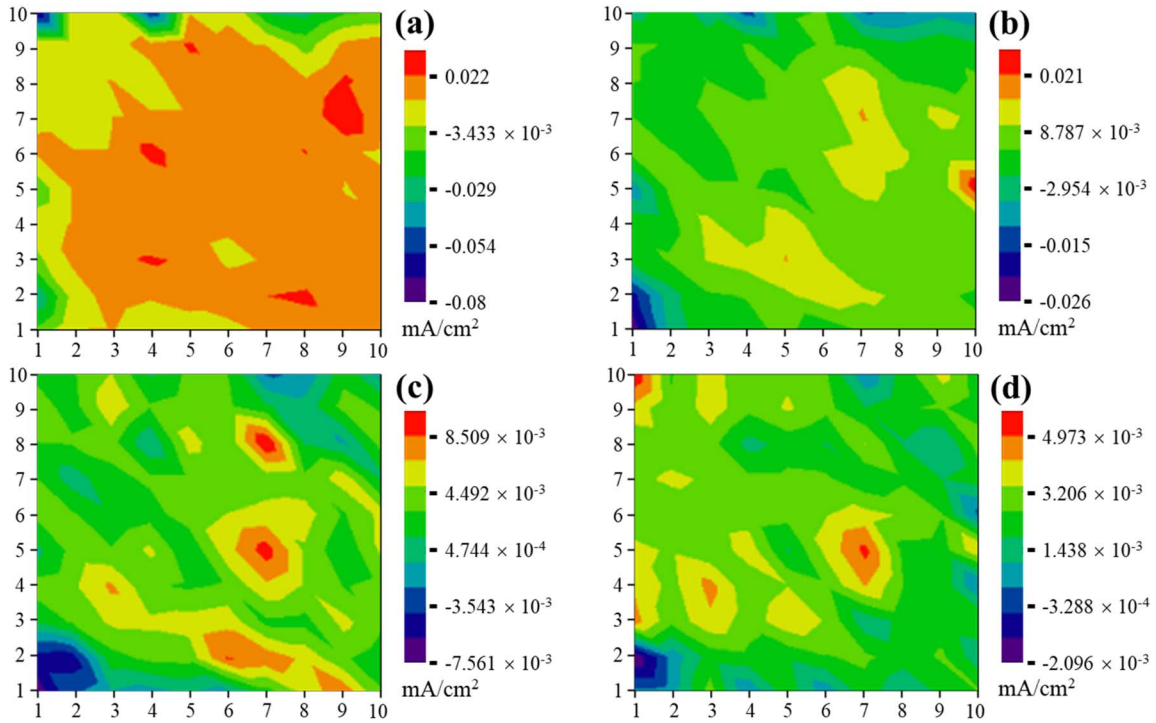

Fig. 8 Galvanic current map distributed to the WBE surface after (a) 1 h immersion in a CO_2-saturated 0.01 M NaCl solution without inhibitor addition and after 24 h with (b) 0.4, (c) 1.2, and (d) 2.4 mM $PrCl_3$ additions.

dissociation of $PrCl_3$ in the investigated solution at pH ~ 4, and subsequently reacted with OH^-, leading to the formation of praseodymium oxides and hydroxides due to the hydrolysis process. The hydrolysis process could be described as follows:[62]

$$[Pr(H_2O)_9]^{3+} + H_2O \rightarrow [Pr(H_2O)_8(OH)]^{2+} + H_3O^+ \quad (1)$$

The process could produce a strong acid and this soluble species can be polymerized to form di- or poly-nuclear species in the investigated solution. Furthermore, the local pH around the cathodic sites of electrochemical corrosion reaction should be increased due to the increase in OH^- generation at these sites on the steel surface. Therefore, when electrochemical corrosion reactions start on the steel surface, the fast diffusion processes happen to equalize the locally strong base (high OH^- concentration) at the cathodic sites and availably strong acid formed in the hydrolysis process. Hence, the praseodymium hydroxide immediately deposits on the top of cathodic sites and this deposit process could continue when other cathodic reactions occur on the steel surface. Meanwhile, this solid protective layer is also promoted by iron oxides, hydroxides and carbonates, which were formed at the anodic sites. These processes could result in the incorporation of the precipitate layer that agrees with other findings,[63,64] producing an entirely deposited steel surface that strongly hinders the electrochemical corrosion. In previous studies, the addition of $LaCl_3$ and $CeCl_3$ into CO_2-saturated NaCl solution resulted in inhibition efficiencies of 95.97 ± 0.41%[65] and 95.86 ± 0.82%,[66] respectively, for the corrosion protection of mild steel. The present work evaluated the performance of $PrCl_3$, which exhibited a higher inhibition efficiency compared with $CeCl_3$ and $LaCl_3$. The difference in inhibition efficiency can be expalined by the intrinsic properties of the Pr^{3+} ion. Firstly, $LaCl_3$ in the corrosive medium exists predominantly in the stable La(III) state, thereby exhibiting a slightly higher efficiency than $CeCl_3$, where the coexistence of Ce(III) and Ce(IV) limits its protective capability. In contrast, although Pr resembles Ce in that both have the +III and +IV oxidation states. This can be explained by the smallest ionic radii of Pr^{3+} (1.13 Å), which enhances surface coverage due to a higher surface coverage. Importantly, despite its larger atomic number, the lanthanide contraction effect further reduces the ionic radius, enabling praseodymium oxides/hydroxides to precipitate at lower solubility and pH thresholds compared with their lanthanum- or cerium-based.[62] Consequently, even with the oxidation state transition between +III and +IV, the resulting Pr-based precipitates exhibit suitable stability and optimal coverage, thereby ensuring superior protection of the mild steel surface.

4. Conclusions

The work has systematically characterized the influences of small amounts of praseodymium(III) chloride from 0.0 to 2.4 mM on the corrosion properties of mild steel in an environment containing carbon dioxide and chloride ions. Ultimately, $PrCl_3$ performs an attractive corrosion resistance for mild steel *via* mitigating both cathodic and anodic processes. The increase in $PrCl_3$ concentration from 0.0 to 2.4 mM promotes inhibition performance due to a strong reduction in

corrosion current density, achieving 96.33 ± 0.47% at 2.4 mM $PrCl_3$. It is consistent with the significant decrease in polarization resistance. Importantly, the addition of $PrCl_3$ significantly reduced localized corrosion on mild steel surface caused by carbon dioxide and chloride ions. The electrochemical corrosion reactions could be inhibited primarily due to the formation of the barrier layer, which was formed by the incorporation of praseodymium oxides/hydroxides and iron oxide and hydroxide depositions. The incorporated layer could prevent aggressive ion attack to the steel surface, resulting in light corrosion being observed on the inhibited steel surface. Therefore, the work suggests a simple way to protect the mild steel against carbon dioxide corrosion. Future work could explore the application of $PrCl_3$ in a wider range of environments, likely in chloride-rich marine atmospheres and high-temperature acidic or alkaline solutions, with varying pH. Investigating $PrCl_3$'s inhibition performance across different material systems, such as stainless steels, aluminum alloys, and coated substrates, could further clarify its versatility and corrosion inhibitory potential. Moreover, combining $PrCl_3$ with other eco-friendly inhibitors to develop multifunctional inhibition systems, studying its long-term stability and assessing its compatibility with sustainable coating technologies, would expand its potential applicability and industrial relevance.

Conflicts of interest

The authors declare that they have no known competing financial interests or personal relationships that could have appeared to influence the work reported in this paper.

Data availability

The data that support the findings of this study are available from one of the corresponding author (Thanh Liem Huynh) upon reasonable request.

Supplementary information is available. See DOI: **https://doi.org/10.1039/d5ra05060j**.

Acknowledgements

The authors are thankful to Dr Nam Nguyen Dang and Miss Thi Nhung Nguyen for their thorough editorial work, discussions, and English correction.

References

1 E. Paul, J. T. Black and A. K. Ronald, *Materials and Processes in Manufacturing*, Wiley, 9th edn, 2003.
2 H. Cather, R. Morris, M. Philip and C. Rose, in *Design Engineering*, Elsevier, 2001, pp. 74–131.
3 P. T. Pedersen, *Engineering*, 2015, **1**, 131–138.
4 Z. F. Yin, W. Z. Zhao, Y. R. Feng and S. D. Zhu, *Corros. Eng., Sci. Technol.*, 2009, **44**, 453–461.
5 K. Xhanari, Y. Wang, Z. Yang and M. Finšgar, *Chem. Rec.*, 2021, **21**, 1845–1875.
6 *The 2023 IMO Strategy on Reduction of GHG Emissions from Ships*, International Maritime Organization, 2023.
7 J. Li, D. Wang and F. Xie, *Eng. Failure Anal.*, 2022, **137**, 106265.
8 A. Kahyarian, M. Achour and S. Nesic, in *Trends in Oil and Gas Corrosion Research and Technologies*, Elsevier, 2017, pp. 149–190.
9 C. Bian, Z. M. Wang, X. Han, C. Chen and J. Zhang, *Corros. Sci.*, 2015, **96**, 42–51.
10 K. Sotoodeh, *Subsea Valves and Actuators for the Oil and Gas Industry*, Elsevier, 2021.
11 S. H. Kim, G. Obulan Subramanian, C. Kim, C. Jang and K. M. Park, *Surf. Coat. Technol.*, 2018, **349**, 415–425.
12 X. Wang, W. L. Xu, Y. Y. Li, Z. N. Jiang, X. Q. Zeng and G. A. Zhang, *J. Colloid Interface Sci.*, 2023, **639**, 107–123.
13 N. D. Nam, Q. V. Bui, M. Mathesh, M. Y. J. Tan and M. Forsyth, *Corros. Sci.*, 2013, **76**, 257–266.
14 A. Sun, G. Cui and Q. Liu, *Colloids Surf., A*, 2023, **664**, 131106.
15 G. Mubarak, C. Verma, I. Barsoum, A. Alfantazi and K. Y. Rhee, *J. Taiwan Inst. Chem. Eng.*, 2023, **150**, 105027.
16 A. Mishra, J. Aslam, C. Verma, M. A. Quraishi and E. E. Ebenso, *J. Taiwan Inst. Chem. Eng.*, 2020, **114**, 341–358.
17 A. I. A. Michael, *Handbook of Corrosion Inhibitors*, Synapse Information Resources Inc., 2011.
18 C. Deng, L. Yang, X. Wu, L. Fu and J. Li, *Russ. J. Phys. Chem. A*, 2023, **97**, 1290–1301.
19 T. Cholidah, L. L. Kusumasari, T. Febriyanti, A. F. M. Firdaus, R. P. N. Fuadi and K. A. Madurani, *Journal of Bio- and Tribo-Corrosion*, 2025, **11**, 8.
20 H. Liu, C. Chen, X. Yuan, Y. Tan, G. Meng, H. Liu and Y. F. Cheng, *Corros. Sci.*, 2022, **203**, 110345.
21 Z. Zheng, J. Hu, N. Eliaz, L. Zhou, X. Yuan and X. Zhong, *Corros. Sci.*, 2022, **194**, 109930.
22 H. Jiang, B. Wang, J. Liu, J. Zhou and C. Liu, *Arabian J. Chem.*, 2023, **16**, 104774.
23 S. Gupta, R. Yazdi, M. Andersson and R. Ambat, *Corros. Eng., Sci. Technol.*, 2023, **58**, 537–548.
24 X. Liu and Y. G. Zheng, *Corros. Eng., Sci. Technol.*, 2008, **43**, 87–92.
25 J. N. da Cunha, B. D. V. Evangelista, A. V. Xavier, T. U. da Silva, S. M. de Oliveira, J. R. de Araújo, B. S. Archanjo, S. de Paula Machado, M. J. C. Rezende, T. das Chagas Almeida, O. R. Mattos and E. D'Elia, *Corros. Sci.*, 2023, **212**, 110907.
26 Q. H. Zhang and N. Xu, *Ind. Crops Prod.*, 2023, **201**, 116883.
27 I. B. Onyeachu, D. S. Chauhan, M. A. Quraishi and I. B. Obot, *Corros. Eng., Sci. Technol.*, 2021, **56**, 154–161.
28 C. Shen, V. Alvarez, J. D. B. Koenig and J.-L. Luo, *Corros. Eng., Sci. Technol.*, 2019, **54**, 444–454.
29 D. Shaikhah, R. Barker, W. Taleb, A. Lazareva, M. Mohamed-Said, B. Cowe and A. Neville, *Polymer*, 2022, **242**, 124614.
30 S. S. Al-Shihry, A. R. Sayed and H. M. Abd El-lateef, *J. Mol. Struct.*, 2020, **1201**, 127223.
31 K. R. Ansari, A. Singh, M. Younas, I. H. Ali and Y. Lin, *Chem. Pap.*, 2024, **78**, 8563–8576.
32 T. Ibrahim, E. Gomes, I. B. Obot, M. Khamis and M. Abou Zour, *J. Adhes. Sci. Technol.*, 2016, **30**, 2523–2543.

33 A. Singh, Y. Lin, W. Liu, D. Kuanhai, J. Pan, B. Huang, C. Ren and D. Zeng, *J. Taiwan Inst. Chem. Eng.*, 2014, **45**, 1918–1926.
34 A. Berisha, E. Krasniqi, J. Halili, K. Jusufi, A. Reka, V. Mehmeti, A. Halili and O. Dagdag, *Chem. Pap.*, 2023, **77**, 6567–6582.
35 O. Agboola, B. Bakre, O. Oladokun, A. O. Ayeni, O. S. I. Fayomi, O. Odunlami, R. Sadiku, A. Adeniyi and P. Popoola, *Chem. Pap.*, 2022, **76**, 5497–5511.
36 Y. Tan, M. Mocerino and T. Paterson, *Corros. Sci.*, 2011, **53**, 2041–2045.
37 X. Liu, P. C. Okafor and Y. G. Zheng, *Corros. Sci.*, 2009, **51**, 744–751.
38 V. C. Anadebe, V. I. Chukwuike, K. Chandra Nayak, E. E. Ebenso and R. Chandra Barik, *Mater. Chem. Phys.*, 2024, **312**, 128606.
39 N. D. Nam, M. Mathesh, B. Hinton, M. J. Y. Tan and M. Forsyth, *J. Electrochem. Soc.*, 2014, **161**, C527–C534.
40 N. D. Nam, C. Panaitescu, M. Y. J. Tan, M. Forsyth and B. Hinton, *J. Electrochem. Soc.*, 2018, **165**, C50–C59.
41 M. Forsyth, M. Seter, M. Y. Tan and B. Hinton, *Corros. Eng., Sci. Technol.*, 2014, **49**, 130–135.
42 G. B. Deacon, M. Forsyth, P. C. Junk, S. G. Leary and W. W. Lee, *Z. Anorg. Allg. Chem.*, 2009, **635**, 833–839.
43 W. Gong, B. Yang, H. Chen, Y. Chen, X. Shen, W. Hao, X. Wang and L. Huang, *Int. J. Electrochem. Sci.*, 2023, **18**, 100242.
44 X. Xing, Z. Han, H. Wang and P. Lu, *J. Rare Earths*, 2015, **33**, 1122–1128.
45 X. Zhang, W. Wei, L. Cheng, J. Liu, K. Wu and M. Liu, *Appl. Surf. Sci.*, 2019, **475**, 83–93.
46 D. Mohammedi, F. Ismail, R. Rehamnia, R. Bensalem and O. Savadogo, *Corros. Eng., Sci. Technol.*, 2015, **50**, 633–638.
47 M. A. El-Hashemy, A. E. Hughes, T. Gengenbach, A. M. Glenn and I. S. Cole, *J. Rare Earths*, 2023, **41**, 309–320.
48 S. J. García, T. H. Muster, Ö. Özkanat, N. Sherman, A. E. Hughes, H. Terryn, J. H. W. de Wit and J. M. C. Mol, *Electrochim. Acta*, 2010, **55**, 2457–2465.
49 H. Allachi, F. Chaouket and K. Draoui, *J. Alloys Compd.*, 2010, **491**, 223–229.
50 H. T. N. Nguyen, N. T. Nguyen, K. L. Duong Ngo, H. B. Do, H. P. Phu Anh, M. Kim, S. V. P. Vattikuti and N. N. Dang, *Ceram. Int.*, 2025, **51**, 37398–37411.
51 P. S. Nial, C. Sathyaseelan, M. M. Bhanjadeo, K. D. Tulsiyan, T. Rathinavelan and U. Subudhi, *J. Mol. Liq.*, 2024, **407**, 125173.
52 M. Jomaa, G. Pelletier, D. Dieme, J. Côté, H. Fetoui, A. Nong and M. Bouchard, *Arch. Toxicol.*, 2023, **97**, 3061–3074.
53 Y. J. Tan, S. Bailey, B. Kinsella and A. Lowe, *J. Electrochem. Soc.*, 2000, **147**, 530.
54 Y. S. Choi and S. Nešić, *Int. J. Greenhouse Gas Control*, 2011, **5**, 788–797.
55 A. Kahyarian, B. Brown and S. Nešić, *Corrosion*, 2018, **74**, 851–859.
56 A. Kahyarian and S. Nesic, *J. Electrochem. Soc.*, 2019, **166**, C3048–C3063.
57 B. Linter and G. Burstein, *Corros. Sci.*, 1999, **41**, 117–139.
58 J. R. MacDonald, *Impedance Spectroscopy*, Wiley, New York, 1987.
59 J. P. Diard, P. Landaud, B. Le Gorrec and C. Montella, *J. Electroanal. Chem. Interfacial Electrochem.*, 1988, **255**, 1–20.
60 D. A. Jones, *Principles and Prevention of Corrosion*, Prentice Hall, Singapore, 1997.
61 J. de Damborenea, A. Conde and M. A. Arenas, in *Rare Earth-Based Corrosion Inhibitors*, Elsevier, 2014, pp. 84–116.
62 G. W. F. A. Cotton, *Advanced Inorganic Chemistry*, Wiley, New York, 1988.
63 M. A. Arenas and J. J. de Damborenea, *Electrochim. Acta*, 2003, **48**, 3693–3698.
64 S. Virtanen, M. B. Ives, G. I. Sproule, P. Schmuki and M. J. Graham, *Corros. Sci.*, 1997, **39**, 1897–1913.
65 T. B. N. Dao, K. L. Duong-Ngo, T. L. Huynh, T. N. Tran, T. T. Pham, M. Kim, T. N. Nguyen and D. N. Nguyen, *Colloids Surf., A*, 2025, **721**, 137208.
66 T.-B.-N. Dao, S. V. Prabhakar Vattikuti, T. T. Pham, C. Panaitescu, N. Q. Tran, K. L. Duong-Ngo and D. N. Nguyen, *Surf. Interfaces*, 2025, **67**, 106564.